Synthetic Amorphous Silica Nanoparticles Promote Human Dendritic Cell Maturation and CD4+ T-Lymphocyte Activation

Alexia Feray, Éléonore Guillet, Natacha Szely, Marie Hullo, François-Xavier Legrand, Emilie Brun, Thierry Rabilloud, Marc Pallardy, Armelle Biola-Vidamment

This is an author version of the paper originally published in Toxicological Sciences under the doi: 10.1093/toxsci/kfab120

Synthetic amorphous silica nanoparticles promote human dendritic cell maturation and CD4 + T-lymphocyte activation

Alexia Feray[1#], Eléonore Guillet[1#], Natacha Szely[1], Marie Hullo[1], François-Xavier Legrand[2], Emilie Brun[3], Thierry Rabilloud[4], Marc Pallardy[1] and Armelle Biola-Vidamment[1,*]

1. Université Paris-Saclay, Inserm, Inflammation, Microbiome and Immunosurveillance, 92290, Châtenay-Malabry, France.

2. Université Paris-Saclay, CNRS, Institut Galien Paris Saclay, 92296, Châtenay-Malabry, France

3. Université Paris-Saclay, CNRS, Institut de Chimie Physique, 91405, Orsay, France.

4. UMR CNRS 5249, Laboratoire de Chimie et Biologie des Métaux, CEA-Grenoble, 17 avenue des Martyrs, 38 054 Grenoble Cedex 09, France.

# co-first authorship. AF and EG contributed equally to this work.
***Corresponding author**: Armelle Biola-Vidamment, INSERM UMR-996, Faculté de pharmacie, Université Paris-Saclay, 5 rue JB Clément, 92296 Chatenay-Malabry cedex, France. Phone: 33-1 46 83 59 80. Fax: 33-1 46 83 54 96. E-mail: armelle.biola-vidamment@universite-paris-saclay.fr.

Keywords amorphous silica nanoparticles, dendritic cells, danger signal, T-lymphocytes, immunotoxicology.

Running head Amorphous SiO_2 nanoparticles activate human dendritic cells

Abstract
Innate immune cells such as dendritic cells (DCs) sense and engulf nanomaterials potentially leading to an adverse immune response. Indeed, as described for combustion-derived particles, nanomaterials could be sensed as danger signals, enabling DCs to undergo a maturation process, migrate to regional lymph nodes and activate naive T-lymphocytes. Synthetic amorphous silica nanoparticles (SAS-NPs) are widely used as food additives, cosmetics, and construction materials. This work aimed to evaluate *in vitro* the effects of manufactured SAS-NPs, produced by thermal or wet routes, on human DCs functions and T-cell activation. Human monocyte-derived DCs (moDCs) were exposed for 16 hours to three endotoxin-free test materials: fumed silica NPs from Sigma-Aldrich (#S5505) or the JRC Nanomaterial Repository (NM-202) and colloidal Ludox®TMA NPs. Cell viability, phenotypical changes, cytokines production, internalization, and allogeneic CD4+ T-cells proliferation were evaluated. Our results showed that all SAS-NPs significantly upregulated the surface expression of CD86 and CD83 activation markers. Secretions of pro-inflammatory cytokines (CXCL-8 and CXCL-12) were significantly enhanced in a dose-dependent manner in the moDCs culture supernatants by all SAS-NPs tested. In an allogeneic co-culture, fumed silica-activated moDCs significantly increased T-lymphocyte proliferation at all T-cell:DC ratios compared to unloaded moDCs. Moreover, analysis of co-culture supernatants regarding the production of T-cell-derived cytokines showed a significant increase of IL-9 and IL-17A and F, as well as an upregulation of IL-5, consistent with the pro-inflammatory phenotype of treated-moDCs. Taken together, these results suggest that SAS-NPs could induce functional moDCs maturation and play a role in the immunization process against environmental antigens.

Impact statement
Synthetic amorphous silica nanoparticles (SAS-NPs) promote the two first steps of adaptive immune response by increasing the maturation of human DCs and triggering a T-lymphocyte response, characterized by increased proliferation and cytokine secretion. SAS-NPs may therefore play a role in the immunization process against environmental antigens, in situations where simultaneous exposure with nanoparticles could occur in the workplace, as well as in everyday life.

1. Introduction

Synthetic amorphous silica nanoparticles (SAS-NPs) are among the three most-produced nanomaterials worldwide and have long been considered highly biocompatible when compared to their crystalline counterparts (Croissant et al. 2020). They are industrially produced by wet (colloidal) or thermal (pyrogenic) routes (Croissant et al. 2020). Fumed silica, a pyrogenic SAS-NPs, is found in everyday products such as cosmetics as an anti-caking or emulsifying agent (Sccs and Hoet 2016) or in dehydrated food as the widespread food additive E 551 (Winkler et al. 2016; Younes et al. 2018). Colloidal SAS-NPs are not authorized as food additives but are nonetheless used in a broad range of industrial applications. In addition to everyday "intentional" exposure, the use of SAS-NPs both in manufacturing processes and more generally in the workplace also raises the issue of the safety of "accidental" exposure, which may depend on the procedures and protective measures implemented. For these reasons, SAS-NPs belong to the OECD list of prioritized engineered nanoparticles having relevance in the workplace.

Pulmonary exposure to SAS-NPs causes a reversible inflammatory response in mice (Arts et al. 2007; Napierska et al. 2010; Sun et al. 2016). Interestingly, repetitive intratracheal instillation of fumed silica every week for 3 consecutive weeks results in profibrotic effects in the lung and biopersistence linked to a defect in lung clearance (Sun et al. 2016). Moreover, ingestion of SAS-NPs provokes intestinal inflammation in rodent models (Jani et al. 1990). Less is known on the potential of these nanomaterials to cause unintended immune responses, either promoting the development of allergic diseases or exacerbating the severity of established allergic conditions (Shannahan and Brown 2014). Several *in vivo* studies in animals suggest that SAS-NPs could act as adjuvants, consistent with the pro-inflammatory effects described above. Indeed, polyethylene glycol-coated 90 nm SAS-NPs promoted allergic airway disease in mice co-exposed to ovalbumin using intranasal instillation during sensitization (Brandenberger et al. 2013). Moreover, intranasal administrations of spherical, mesoporous, and pegylated SAS-NPs in mice showed an adjuvant effect in a model of ovalbumin-induced allergic airway inflammation with higher cytokines levels (IL-5, IL-13, IL-1β and IFN-γ) and enhanced inflammatory cell infiltration in broncho-alveolar lavage fluid (Han et al. 2016).

Phagocytic cells such as macrophages and dendritic cells (DCs) are among the first immune cell types to uptake and process nanoparticles (Gustafson et al. 2015). DCs are professional antigen-presenting cells that reside in non-lymphoid tissues in an immature antigen-capturing state. Located at the gates of antigen entry, DCs are constantly sampling their environment. Intestinal, skin, and pulmonary DCs, predominantly located underneath the epithelial basement membrane, sense and capture antigens and present sampled antigens to T-lymphocytes. However, depending on the cellular microenvironment and its effect on DC phenotype, the consequence can be either an immunogenic or a tolerogenic immune response (Lutz and Schuler 2002; Tan and O'Neill 2005).

The presence of various stimuli such as "danger signals" in the microcellular environment (Gallo and Gallucci 2013), causes DCs to undergo a maturation process resulting in the up-regulation of major histocompatibility complex class II (MHC II), co-stimulatory molecules, cytokines and chemokine receptors. DCs then migrate to regional lymph nodes to present the antigen and to activate specific naive T-lymphocytes (Worbs et al. 2017). Classic danger signals are either derived from pathogens and released during infections (Pathogen-Associated Molecular patterns, PAMPs) or result from tissue damages and necrotic dying cells (Damage-Associated Molecular Patterns, DAMPs) (Pradeu and Cooper 2012). But there are newly emerging danger signals, among which man-made nanomaterials, which may activate DCs in aseptic conditions in a similar manner to the microbial molecular patterns (Fadeel 2012; Pallardy et al. 2017). These are designated as NAMPs (Nanoparticles-Associated Molecular Patterns) (Farrera and Fadeel 2015; Gallo and Gallucci 2013).

In vitro studies have explored the danger signal effects of SAS-NPs by focusing on the activation of key immune cells such as DCs. For example, increased activation of murine bone-marrow DCs (BMDCs) with CD86 and MHC II upregulation along with the production of IL-1β (Winter et al. 2011) and TNF-α pro-inflammatory cytokines (Kang and Lim 2012) have both been demonstrated. More recently, internalization of food-grade fumed silica nanoparticles was evidenced in murine steady-state DCs, as well as secretion of IL-1β in a MyD88-dependent mechanism (Winkler et al. 2017). But few studies have been performed using human DCs, and reports addressing DC-phenotypic

changes upon exposure to NPs and functional consequences on the immune system are needed (Barillet et al. 2019; Vallhov et al. 2007; Vallhov et al. 2012).
Understand how SAS-NPs could participate in inappropriate activation of the immune system and establish pertinent *in vitro* endpoints for robust immunotoxicological evaluation of nanomaterials is essential. This work aims to evaluate the effects of relevant pyrogenic or colloidal SAS-NPs on human DCs expression of maturation markers and cytokine secretion and to address the consequences on the T-cell response.

2. Materials and methods

2.1. Reagents and materials

The fumed silica NPs mainly used in this work were commercially available (S5505, Sigma-Aldrich, St Quentin Fallavier, France, batch SLBR6988V). According to the manufacturer, their specific surface determined by BET (Brunauer-Emmett-Teller), is 196 $m^2.g^{-1}$. The NPs suspension was prepared from fumed silica dry powder dispersed in filtered ultrapure water at a final concentration of 50 $mg.mL^{-1}$. The suspension was then left for 8 hours in a water bath at 80 °C to sterilize the suspension. The absence of bacterial growth in the nanoparticle's suspension was checked after the process, and a LAL test was performed on each batch to address endotoxin contamination. Before each experiment, an intermediate dilution at a concentration of 500 $\mu g.mL^{-1}$ was prepared in RPMI 1640 medium supplemented with Glutamax, 1mM sodium pyruvate, 0.1 $ng.mL^{-1}$ streptomycin, and 100 $U.mL^{-1}$ penicillin (Gibco, Invitrogen, Saint Aubin, France). The suspension was sonicated for 15 minutes before DCs treatment. The SiO_2-NM202-JRCNM02002 (vial JRCNM02002a990868) was obtained from the European Commission, Joint Research Center JRC Nanomaterial Repository, Ispra, Italy. NM-202 NPs are produced via a high-temperature process and have been thoroughly characterized as they are used as benchmark materials, representative of the nanosized fraction of silicon dioxide contained in the E551 food additive. Their specific surface determined by BET is 204 $m^2.g^{-1}$.The suspension was dispersed in filtered ultrapure water at a final concentration of 1 $mg.mL^{-1}$ and sterilized as previously described for S5505. The Ludox® TMA NPs (420859, Sigma-Aldrich, St Quentin Fallavier, France, batch MKBV6154V) is an aqueous dispersion of negatively charged silica particles with a particle size of 22 nm and not stabilized by a counter ion. They display a specific surface of 134 $m^2.g^{-1}$ and are supplied as a 34% suspension in water and stored at room temperature. Ludox® TMA NPs are sonicated in an ultrasound bath for 15 minutes before use and then vortexed and diluted to the desired concentration in fetal calf serum-free culture medium.

2.2. Characterization of synthetic amorphous silica nanoparticles

The hydrodynamic diameter of particles was determined at 25°C by Dynamic Light Scattering (DLS) using a Zetasizer Nano ZS 90 (Malvern Instruments, Orsay, France) operating at a fixed scattering angle at 90° and equipped with a Helium-Neon laser source with a wavelength of 633 nm. Measurements were performed in disposable 4-mL cuvettes with 1-cm optical pathway and four optical faces (Sarstedt, Marnay, France) containing an appropriate volume (1 mL) of the sample, prepared as described above, after dilution to 125 $\mu g.mL^{-1}$ in the desired medium. The hydrodynamic diameter values were calculated using the Stokes-Einstein equation assuming a spherical shape of the particles. The particle size profile was obtained from the intensity-weighted distribution and the hydrodynamic diameter value corresponds to the median diameter derived from the cumulative distribution curve. The □-potential measurements were carried out with the same instrument at 25°C by laser doppler velocimetry at a detection angle of 17° in DTS 1060 disposable cells (Malvern Instruments, Orsay, France) loaded with approximately 1 mL of each sample diluted to 375 $\mu g.mL^{-1}$ in the desired medium. Due to the ionic strength of the samples leading to high conductivity, measurements were performed using the monomodal mode and the Smoluchowski approximation was used to convert the electrophoretic mobility to □-potential. Values are given as mean values of ten measurements. We carried out the characterization before and after heating at 80°C. The results (DLS and zeta potential) showed no significant difference, confirming that sterilization does not alter the physicochemical characteristics of fumed silica nanoparticles (data not shown).
For transmission electron microscopy experiments, 2 µL of 1 $mg.mL^{-1}$ aqueous suspension of NPs was deposited onto a formvar/carbon-coated copper grid and observed using a JEOL 1400

transmission electron microscopy (TEM) instrument (JEOL Ltd, Tokyo, Japan) operating at 120 kV. Analysis of recorded images was performed using the FIJI (Schindelin et al. 2012).

2.3. Endotoxin detection

Possible endotoxin contamination was analyzed with the Limulus amebocyte lysate (LAL) assay (GenScript, Piscataway, NJ, USA). All batches showed values below the threshold of endotoxin positivity (0.05 $EU.mL^{-1}$).

2.4. Generation of primary cultures of human moDCs

Human monocyte-derived dendritic cells (moDCs) were derived from monocytes isolated from human peripheral blood supplied by the French Blood Bank (EFS, Rungis, France). Healthy donors gave their written consent for the use of blood donation for research purposes. Peripheral blood mononuclear cells (PBMCs) were sorted from buffy coats by density centrifugation on a Ficoll gradient. Monocytes were then isolated through positive magnetic selection using MidiMacs separation columns and anti-CD14+ antibodies coated on magnetic beads (Miltenyi Biotec, Bergisch Gladbach, Germany). Finally, CD14+ cells were differentiated in immature moDCs for 4 days in RPMI 1640 supplemented with GlutaMAX (Gibco, Invitrogen, Saint Aubin, France), 10 % heat-inactivated fetal bovine serum (FBS, Gibco, Invitrogen, Saint Aubin, France), 550 $U.mL^{-1}$ granulocyte-macrophage colony-stimulating factor (rh-GM-CSF, Miltenyi Biotec, Bergisch Gladbach, Germany), 550 $U.mL^{-1}$ interleukin-4 (rh-IL4, Miltenyi Biotec, Bergisch Gladbach, Germany), 1 mM sodium pyruvate (Gibco, Invitrogen, Saint Aubin, France), 100 $\mu g.mL^{-1}$ streptomycin and 100 $U \cdot mL^{-1}$ penicillin (Gibco, Invitrogen, Saint Aubin, France).

2.5. In vitro exposure of immature moDCs to synthetic amorphous silica nanoparticles

After proper differentiation, immature human moDCs were collected, washed, and resuspended in a fresh complete culture medium (RPMI supplemented with 10 % FBS, 1 mM sodium pyruvate, 0.1 $ng.mL^{-1}$ streptomycin, and 100 $U.mL^{-1}$ penicillin) at a final density of 10^6 $cells.mL^{-1}$. Cells were then exposed 16 hours either to 0, 12.5, 25 or 50 $\mu g.mL^{-1}$ of sonicated SAS-NPs (fumed silica S5505, Ludox® TMA, NM-202) or to 25 $ng.mL^{-1}$ of lipopolysaccharide (LPS, ref: L6529, Escherichia coli, serotype 055-B5, Sigma-Aldrich, St Quentin Fallavier, France) as a positive control of moDCs activation. Cells were exposed in the absence of FBS for the first hour of exposition to minimize the impact of serum proteins. Then, the medium was returned to 10% FBS for the proper survival of the cells during the next 15 hours.

2.6. Cytotoxicity assay

Viability was assessed by labeling with propidium iodide (PI, Invitrogen, Saint Aubin, France). After treatment with SAS-NPs at 0, 12.5, 25, or 50 $\mu g.mL^{-1}$, cells were washed with PBS and incubated with PI at 6.25 $mg.L^{-1}$, and the percentage of viability was measured by flow cytometry. We previously tested that under these experimental conditions, SAS-NPS did not interfere with the result of the cytotoxicity test.

2.7. Phenotypic analysis

To assess the effects of SAS-NPs exposure on moDCs phenotype, several surface maturation markers were studied. After 16 hours of exposure to either 0, 12.5, 25, or 50 $\mu g.mL^{-1}$ SAS-NPs or 25 $ng.mL^{-1}$ LPS, moDCs were collected, washed with PBS, and incubated for 20 minutes either with fluorochrome-conjugated monoclonal antibodies (mAbs) or with appropriate isotype control antibodies (IgGs). The following mAbs were used: CD80 (FITC-Mouse anti-human CD80/FITC Mouse IgG1 Isotype control, BD Biosciences, Le Pont de Claix, France), CD83 (PE-Mouse anti-human CD83/PE Mouse IgG1 Isotype control, BD Biosciences, Le Pont de Claix, France), CD86 (APC-Mouse anti-human CD86/APC Mouse IgG1 Isotype control, BD Biosciences, Le Pont de Claix, France), CXCR-4 (APC Mouse anti-human CD184/APC Mouse IgG1 Isotype control, BD Biosciences, Le Pont de Claix, France), CD40 (FITC-Mouse anti-human CD40/FITC Mouse IgG1 Isotype control, BD Biosciences, Le Pont de Claix, France) and PDL-1 (FITC-Mouse anti-human CD274/FITC Mouse IgG1 Isotype control, BD Biosciences, Le Pont de Claix, France). After incubation, moDCs were washed with PBS and then analyzed on a FACS Attune NxT® acoustic

focusing cytometer (ThermoFisher Scientific, Waltham, MA, USA). Results were expressed as the fold increase of the percentage of the positive cells compared to control (untreated moDCs).

2.8. Internalization of nanoparticles by moDCs

After NP exposure (as described above), cells were rinsed with PBS, fixed in 2.5% glutaraldehyde 2% PFA in cacodylate buffer (0.1 M pH 7.4) for 1h30 at room temperature, then rinsed with cacodylate buffer. Post-fixation was achieved in 1% osmium tetroxide 1.5 % potassium ferrocyanide solution at room temperature for one hour. After extensive washings with water, pellets were included in 2% LMP agarose and cut in mm^3 blocks. They were dehydrated through a graded series of ethanol before being embedded in Epon resin. Ultra-thin sections of 70 nm were cut with an EM UC6 ultramicrotome (Leica Microsystems) and stained for 10 min with 2% uranyl acetate (Merck) and 3 min with Reynolds lead citrate (Agar). They were then observed in TEM with a JEOL JEM-1400 electron microscope operating at 120 kV.

2.9. Co-culture of moDCs and CD4+ T-cells

As previously described (Feray et al. 2020), CD4+ T-cells were isolated from PBMC by positive selection with midiMACS separation columns and anti-CD4 antibodies coated on magnetic beads (Miltenyi Biotec, Bergisch Gladbach, Germany). These T-cells were confirmed to have purity greater than 95%, based on CD4 expression evaluated by flow cytometry (561841, RPA-T4, BD Biosciences, Le Pont de Claix, France). CD4+ T-lymphocytes were labeled with 0.5 mM carboxyfluorescein succinimidyl ester (CFSE, Invitrogen, Saint Aubin, France), following the manufacturer's instruction. MoDCs were stimulated by 0, 12.5 or 25 $\mu g.mL^{-1}$ of S5505 fumed silica NPs or 25 $ng.mL^{-1}$ of LPS (positive control for danger signal effects) for 16 hours and then washed and co-cultured with allogeneic CD4+ T-cells at a 1:20 (1 moDC for 20 CD4+ T-cells), 1:50 (1 moDC for 50 CD4+ T-cells) or 1:100 (1 moDC for 100 CD4+ T-cells) DC:T-cell ratio for five days, in RPMI 1640 Glutamax (Gibco, Invitrogen, Saint Aubin, France) supplemented with 10% FBS in round-bottom 96 well plates (Cellstar, Greiner bio-one, Courtaboeuf, France) as previously described (Feray et al. 2020). A DC:T-cell co-culture loaded with the mitogen phytohaemagglutinin (PHA, Invitrogen, Saint Aubin, France) was used as a positive control for T-cell proliferation. Analysis of T-cell proliferation was assessed as the $CFSE_{low}$ cells by flow cytometry, on a FACS Attune NxT® acoustic focusing cytometer (ThermoFisher Scientific, Waltham, MA, USA).

2.10. Cytokine quantification in cell culture supernatants

MoDCs mono- or co-culture supernatants were measured in duplicate for IL-1β, IL-6, CXCL-8, IL-12p40, CCL-2 (MCP-1), CXCL-12 and CXCL-10 (IP-10), IL-17A, IL-17F, IL-5, IL-13, IL-9, IFN-□, IL-10 and IL-22 using Meso Scale Discovery multiplex assay (MSD, Rockville, MA, USA) following manufacturer's instructions.

3. Results

3.1. Characterization of synthetic amorphous silica nanoparticles

Silica exists in a multitude of different forms for industrial applications. SAS-NPs are synthesized through low-temperature colloidal or high-temperature pyrolysis routes (Croissant et al. 2020). In this study, we mainly focused on two fumed silica NPs (commercially available S5505 and NM-202 benchmark material). For comparison, Ludox® TMA NPs were also studied.

Transmission electron microscopy (TEM) is among the gold-standard method for NPs characterization as it allows the assessment of the morphology and external dimensions of the constituent particles. S5505 fumed silica or Ludox® TMA NPs dispersed in water were deposited onto TEM grids for analysis (figure S1A and B). S5505 fumed silica NPs were rounded-shaped and appeared fused as chain-like structures (figure S1A). The median diameter of the identifiable constituent nanoparticles was 14.4 ± 5.3 nm (figure S1B) which is in the same range as the values determined by Sun *et al.* (Sun et al. 2016) and by Winkler *et al.* (Winkler et al. 2017). According to DLS measurements, which are based on Brownian motion (figure S1C), S5505 fumed silica in RPMI 1640 medium led to a bimodal distribution with a first main population centered on 123 ± 53 nm and a second one on 8.7 ± 0.3 µm, testifying of agglomeration and/or aggregation processes. The addition of 1% of FBS to the medium

also led to a bimodal distribution. However, the size corresponding to the first main population increased to 2.2 ± 1.1 µm while the second population remained unchanged (hydrodynamic diameter close to 8.5 ± 0.8 µm). Supplementation with 10% FBS did not greatly change the sizes of the two populations (1.5 ± 0.6 µm and 7.7 ± 1.9 µm) but led to an increase in the proportion of the second population. Optical microscopy, and in particular granulomorphometry (data not shown), was used to search for additional details but the contrast between the particles and the buffer was weak in the same manner as previously described by Doi (Doi 1982). The □-potential value for S5505 in RPMI 1640 was -22.5 ± 1.4 mV and increased to -13.5 ± 1.5 mV and to -8.5 ± 1.9 mV in presence of 1% and 10% of FBS respectively (figure S1D). This increase, even at low serum concentration, suggests that a protein layer is formed on particles (Monopoli et al. 2011). It should be noted that the sterilization step at 80°C for 8 hours does not modify the size and □-potential behavior of S5505 fumed silica (data not shown) as the same tendency was observed with or without FBS.
Regarding NM-202 DLS size measurements, two peaks were observed in pure RPMI 1640 at 160 ± 33 nm and 8.9 ± 0.5 µm, showing similar behavior to fumed silica (figure S1C). The addition of 10% of FBS led to an increase in the first population to 423 ± 189 nm while the second population remained unchanged (hydrodynamic diameter close to 7.0 ± 3.2 µm). Moreover, free serum proteins were detected at 7.4 ± 1.0 nm. The □-potential values for NM-202 nanoparticles were equal to -20.1 ± 0.5 mV and -6.9 ± 0.5 mV in absence of FBS and with 10% of FBS respectively (figure S1D), confirming adsorption of FBS components to the particle surface as for S5505 fumed silica NPs.
As for Ludox® TMA NPs, they present higher size and shape homogeneities according to TEM images (figures S1A and B). Their median diameter determined by TEM was 16.5 ± 2.0 nm (figure S1B) which is lower than the median hydrodynamic diameter measured by DLS (27.2 ± 0.3 nm) (figure S1C). This phenomenon is classic as the dispersion of NPs into an electrolyte led to a layer on the surface, measured by DLS, which is composed of ions and molecules of the dispersion medium. Supplementation with 1% of FBS led to a bimodal distribution with a first large population centered on 50.8 ± 4.3 nm and a second one at 7.8 ± 0.4 □m bearing out an agglomeration/aggregation (figure S1C). The addition of 10% of FBS to the medium led to a trimodal distribution. The sizes corresponding to the two previous populations remained unchanged (hydrodynamic diameters close to 48.8 ± 7.5 nm and to 8.6 ± 0.5 □m respectively) while a new population was detected at 144 ± 31 nm corroborating the agglomeration/aggregation mechanism (figure S1C). This phenomenon can be explained by the adsorption of serum proteins at the particle surface. Indeed, □-potential measurements have shown an increase in □-potential in the presence of FBS, this phenomenon is all the more pronounced as there is a high content of FBS (figure S1D).
Thus, as expected given their synthesis routes, fumed silica S5505 and NM-202 NPs have comparable physico-chemical properties while differing from Ludox® TMA NPs.

3.2. Cytotoxicity of synthetic amorphous silica nanoparticles

Phagocytic cells, such as DCs, are suspected to be sensitive to NPs cytotoxicity because of their capability to attain a large intracellular load. To analyze the cytotoxicity of SAS-NPs, human moDCs were incubated for 16 hours with 12.5, 25, 50, or 100 µg.mL^{-1} of S5505 or NM-202 fumed silica or Ludox® TMA NPs. Cell viability was then analyzed by flow cytometry using PI staining. Results showed that all SAS-NPs decreased moDCs viability in a concentration-dependent manner (figure 1). The 50 µg.mL^{-1} concentration of S5505 NPs and 100 µg.mL^{-1} of Ludox® TMA were highly cytotoxic with a 60% cell mortality. Both the 12.5 and 25 µg.mL^{-1} concentrations of S5505 or NM-202 fumed silica (figure 1A and B) and 25 and 50 µg.mL^{-1} of Ludox® TMA NPs (figure 1C) were below or slightly above the 30% cytotoxicity established threshold and were retained for further experiments. These cytotoxicity results led us to select different working concentrations for each type of nanoparticle, so as not to exceed the 30% cytotoxicity threshold. Moreover, based on a sensitive LAL assay, all SAS-NPs tested were below the threshold of endotoxin positivity (0.05 EU.mL^{-1}) (figure 1D).

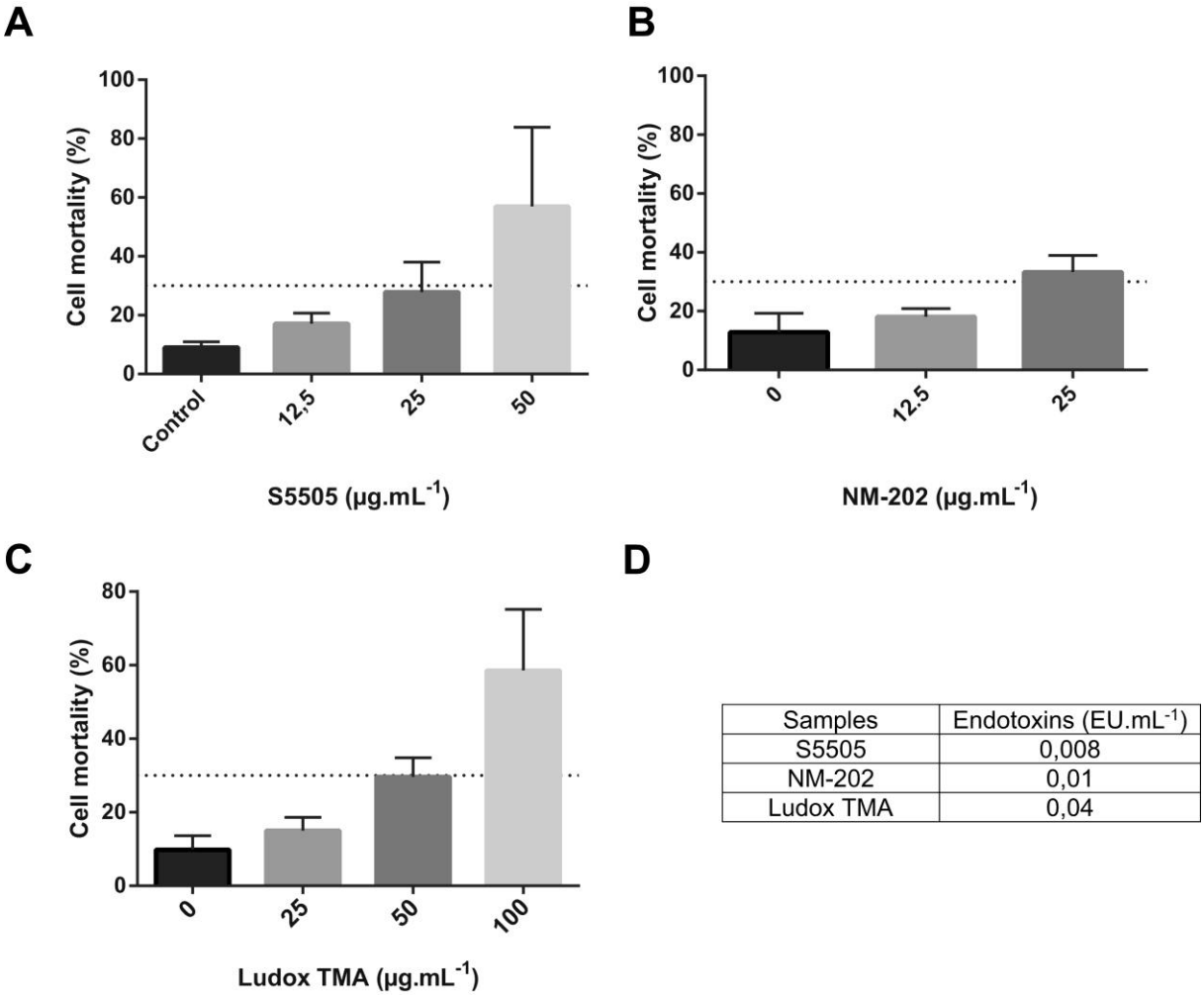

Samples	Endotoxins (EU.mL^{-1})
S5505	0,008
NM-202	0,01
Ludox TMA	0,04

Figure 1. Cytotoxicity and endotoxin levels of synthetic amorphous silica nanoparticles
MoDCs were incubated with 12.5, 25 and 50 µg.mL^{-1} of S5505 fumed silica NPs **(A)** or 12.5 and 25 µg.mL^{-1} of NM-202 NPs **(B)** or 0, 25, 50 or 100 µg.mL^{-1} of Ludox® TMA nanoparticles **(C)** for 16 hours. Cells were then collected, washed and cell viability analyzed by flow cytometry using propidium iodide staining. Results were expressed in percentage of cell mortality and represented the mean ± SEM of three independent experiments. *: $p < 0.05$, **: $p < 0.01$, ***: $p < 0.001$, one-way ANOVA and Tukey's multiple comparison test. **(D)** Endotoxin levels were analyzed with the Limulus amebocyte lysate (LAL) assay. Representative results. The limit of detection was 0.01 EU.mL^{-1} and the threshold of endotoxin positivity was 0.05 EU.mL^{-1}.

3.3. Synthetic amorphous silica nanoparticles modulated moDCs phenotype.

To examine the phenotypic changes of moDCs, cells were incubated with 12.5 and 25 µg.mL^{-1} of S5505 or NM-202 fumed silica NPs, or 25 and 50 µg.mL^{-1} of Ludox® TMA. LPS was used as a positive control for moDCs maturation. The maturation status of the moDCs was then assessed using FACS analysis and measurement of CD80, CD86, CD83, CD40, CXCR4, and PDL-1 expressions. Interestingly, expressions of CD83 and CD86 molecules increased in a dose-dependent manner reaching statistical significance for 25 µg.mL^{-1} of S5505 and NM-202 NPs (figure 2A and B) and 50 µg.mL^{-1} of Ludox® TMA (figure 2C). The expression of CXCR-4 was significantly induced by 25 µg.mL^{-1} of S5505 and 50 µg.mL^{-1} of Ludox® TMA NPs (figures 2A and C). CD40 and PDL-1 expressions were also slightly augmented but did not reach statistical significance. Taken together, our findings suggested that all SAS-NPs tested, whether produced via thermal or wet processes, significantly affected moDCs maturation through up-regulation of the same markers.

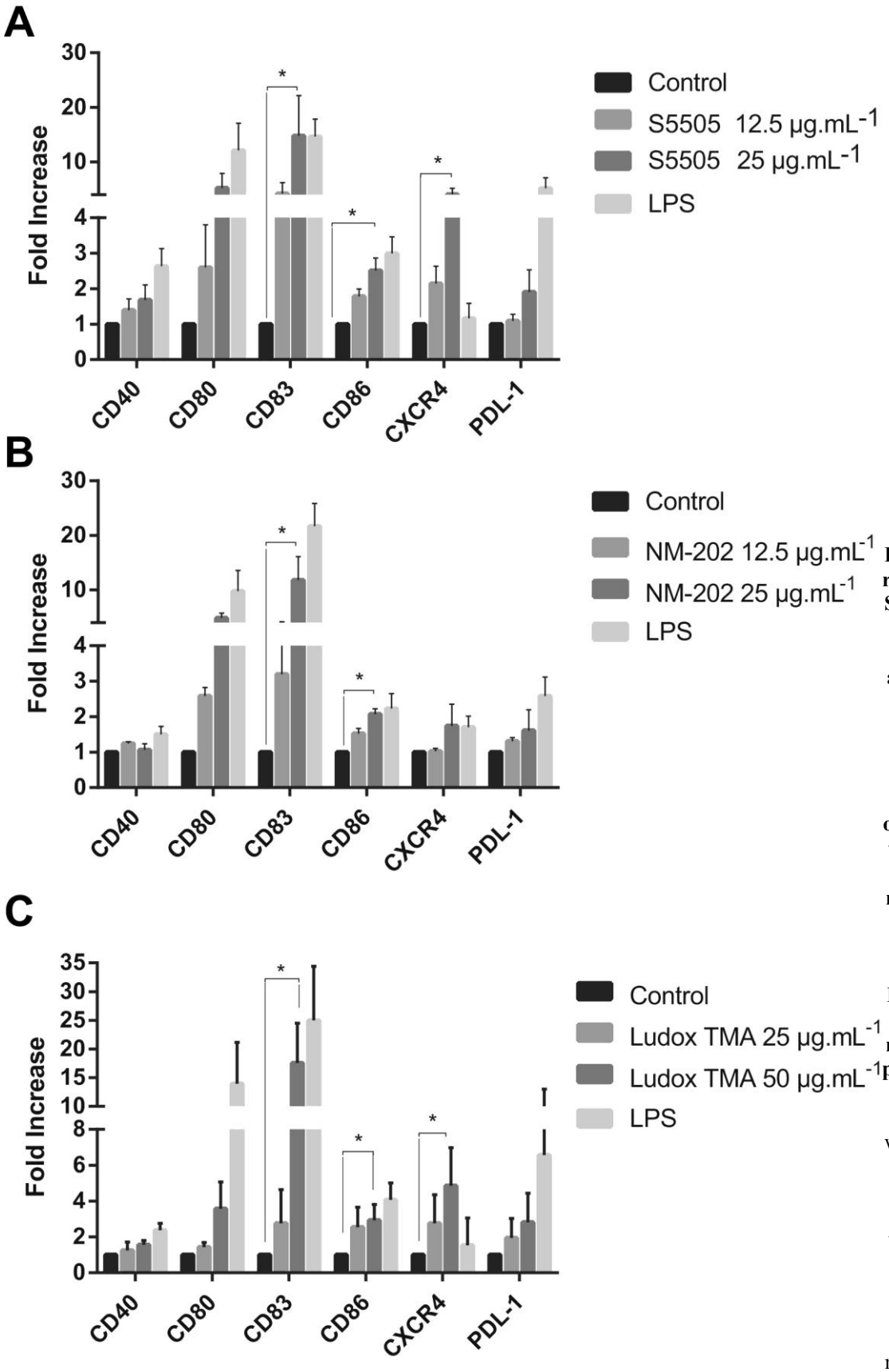

Figure 2. Synthetic amorphous silica nanoparticles modulated moDCs phenotype Cells were incubated with 12.5 and 25 µg.mL^{-1} of S5505 fumed silica nanoparticles (A) or NM-202 (B) or Ludox® TMA (C) for 16 hours. LPS was used as a positive control. Cells were then collected, washed and the maturation status of the moDCs was assessed by

FACS analysis. Unloaded moDCs were used as control. Results were expressed as a fold increase of the percentage of positive cells compared to untreated cells and represented the mean ± SEM of three independent experiments. *: $p < 0.05$ one-way ANOVA and Tukey's multiple comparison test (statistics for LPS are not shown).

3.4.Synthetic amorphous silica nanoparticles induced the production of pro-inflammatory cytokines and chemokines by moDCs

To further document the effect of SAS-NPs on human moDCs phenotype, we assessed the production of pro-inflammatory cytokines and chemokines from particles-treated cells. Again, moDCs were exposed to 12.5, 25, or 50 µg.mL^{-1} of SAS-NPS. The moDCs culture supernatants were collected and analyzed using U-PLEX MSD technology for IL-1β, IL-6, CXCL-8, IL-23, CCL-2 (MCP-1), CXCL-12, CXCL-10 (IP-10), and TNF-α production. Interestingly, secretions of CXCL-8 and CXCL-12 were significantly enhanced in a concentration-dependent manner in the presence of 12.5 to 25 µg.mL^{-1} of S5505 and NM-202 fumed silica NPs (figure 3A and B), as well as 25 and 50 µg.mL^{-1} of Ludox® TMA (figure 3C). Noticeably, IL-6 and CXCL-10 were also significantly upregulated by both concentrations of NM-202 (figure 3B). IL-1□, IL-23, and TNF-α secretions were slightly augmented but did not reach significance (figure S2). From these results, we showed that all SAS-NPs tested were able to increase the production of pro-inflammatory cytokines and chemokines by moDCs, suggesting the existence of an inflammatory signature.

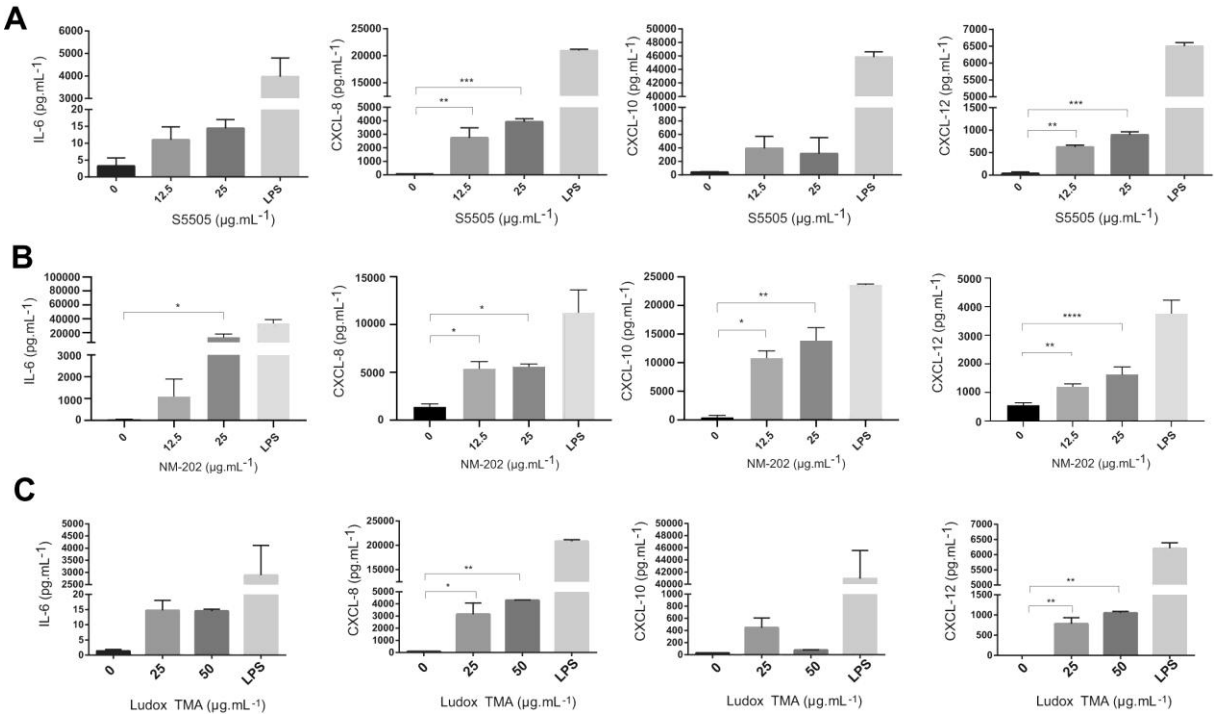

Figure 3. Synthetic amorphous silica nanoparticles induced moDCs inflammatory cytokines and chemokines secretion

Cells were incubated with 12.5 and 25 µg.mL^{-1} of S5505 fumed silica nanoparticles **(A)** or NM-202 **(B)** or Ludox® TMA **(C)** for 16 hours. LPS was used as a positive control. The moDCs culture supernatants were collected and analyzed using U-PLEX MSD technology. Unloaded moDCs were used as control. Results were expressed in the quantity of detected cytokines (pg.mL^{-1}) and represented the mean ± SEM of three independent experiments. **: $p < 0.01$, ***: $p < 0.001$, ****: $p < 0.0001$, one-way ANOVA and Tukey's multiple comparison test (statistics for LPS are not shown).

3.5. Human moDC internalized S5505 fumed silica nanoparticles

To investigate the potential uptake of nanoparticles by moDCs, we performed transmission electron microscopy (TEM) observations. This technique allows to visualize cellular compartments at a nanometer scale and discriminates internalization from membrane adsorption. We focused on S5505 fumed silica which gave comparable results with the benchmark material NM-202 for DC maturation. Control immature DCs were mostly roundly shaped (figure 4A and E). In treated cells, NPs can be observed outside, nearby, and inside DCs. In figure 4B and F, two representative images of S5505 fumed silica-treated cells are shown, as well as higher magnifications depicted by the selection squares (figures C and D for B, G and H for F). Interestingly, SAS-NPs aggregates are present close to the plasma membrane (white arrows) and could be visualized inside cytoplasmic vesicles (black arrows). Intracellular "free" cytoplasmic SAS-NPs aggregates were not detected. Interestingly, SAS-NPs were sometimes partially surrounded by the membrane or dendrites (arrowheads), suggesting an ongoing process of trapping in endocytic vesicles (figures 4C and D). Moreover, after NP exposure, cells tend to present more numerous and longer arborizing dendrites, consistent with an NPs-driven shift of MoDCs maturation.

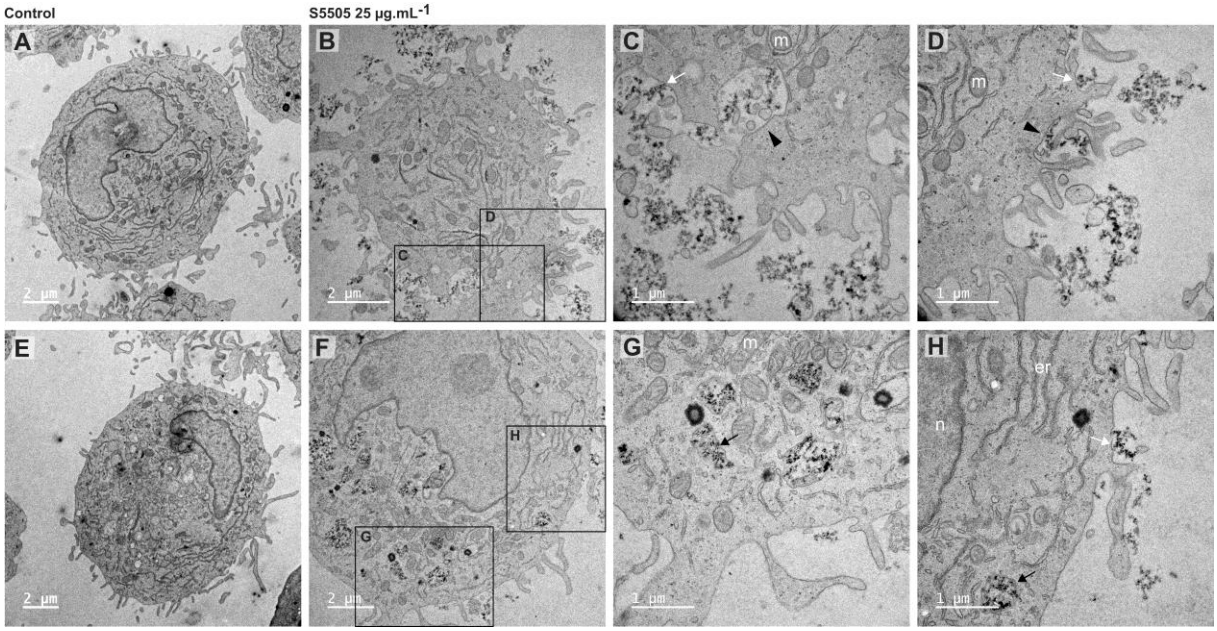

Figure 4. MoDCs treated with S5505 fumed silica nanoparticles showed membrane-wrapped aggregates and vesicular uptake of NPs

Cells were incubated with 25 µg.mL^{-1} of S5505 fumed silica nanoparticles for 24 hours or left untreated.

A, E: untreated MoDCs. B, F: MoDCs incubated with 25 µg.mL-1 of S5505 fumed silica NPs for 24 hours. C, D: magnified images of B. G, H: magnified images of F. Cytoplasmic vesicles containing SAS-NPs (black arrows), SAS-NPs close to the plasma membrane (white arrows), SAS-NPs partially surrounded by the membrane or dendrites (arrowheads). Designations: m, mitochondria; n, nucleus; er, endoplasmic reticulum. Scale bars correspond to 2 µm (A, B, E, F) or 1 µm (C, D, G, H).

3.6. MoDCs stimulated with S5505 fumed silica nanoparticles enhanced CD4+ T-cell proliferation.

To evaluate the functional consequences of moDCs maturation, we analyzed the capacity of moDCs treated with S5505 fumed silica to augment allogeneic CD4+ T-cell proliferation. To limit the cytotoxicity induced by NPs during the allogeneic co-culture, we decided to expose moDCs at the lowest concentration (12.5 µg.mL^{-1}) of S5505 NPs. Treated moDCs were then washed and co-cultured with allogeneic CD4+ T-cells loaded with CFSE at several DC:T-cell ratios. Proliferation was assessed after five days of co-culture as the percentage of $CFSE_{low}$ CD4+ T-cells. A DC:T-cell co-culture stimulated with PHA was used as a positive control for T-cell proliferation and LPS-treated moDCs as a positive control for danger signal effects. The proliferation of T-cells not exposed to DCs was comparable to the background noise (figure 5A). Using a 1:20 DC:T-cell ratio, the addition of non-treated allogeneic moDCs induced a basal T-cell proliferation of about 30% that was statistically

increased by the exposure of moDCs to S5505 NPs (figure 5A). Interestingly, T-cell proliferation levels triggered by S5505 NPs were comparable with those induced by LPS, a well-known danger signal (figure 5A).

Among the variables that regulate the activation of CD4+ T-cells by DCs, the maturation state of the DCs and the relative amounts of stimulating moDCs and responding CD4 + T-cells are of particular importance (Hopken et al. 2005). As previously described, the use of several DC:T-cell ratios is particularly important to confirm the NPs effect and to increase the sensitivity of the method (Feray et al. 2020). We therefore tested the following ratios: 1:100 (corresponding to 1 moDC per 100 T-cells), 1:50 (1 moDC for 50 T-cells) and 1:20 (1 moDC for 20 T-cells). We observed that reducing the DC:T-cell ratios from 1:20 to 1:100 decreased basal proliferation (figure 5B). Consequently, T-cells showed a higher index of proliferation when moDCs were stimulated with S5505 SAS-NPs. The increase in T-lymphocytes proliferation in presence of SAS-NPs-treated moDCs was statistically significant for all tested ratios compared to unloaded moDCs (figure 5B).

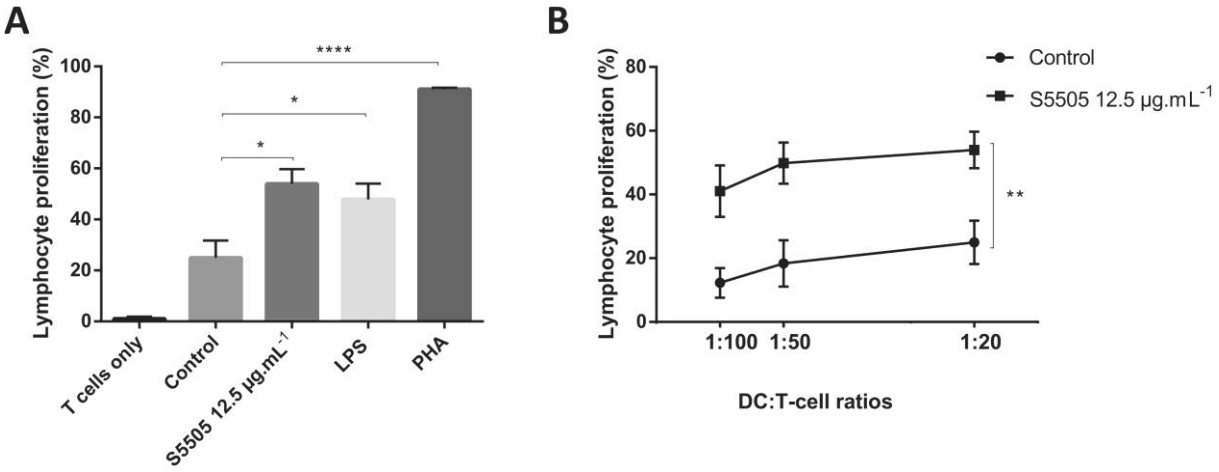

Figure 5. MoDCs treated with S5505 fumed silica nanoparticles increased allogeneic T-cell proliferation

A. Cells were incubated with 12.5 µg.mL^{-1} of S5505 fumed silica nanoparticles for 16 hours. LPS and PHA were used as positive controls. Treated moDCs were co-cultured with allogeneic CD4+ T-cells loaded with CFSE at a ratio of 1 moDC for 20 CD4+ T-cells. Proliferation was measured after 5 days of co-culture as the percentage of CFSE^{low} CD4+ T-cells. Untreated moDCs were used as control. Results were expressed as a percentage of increase in lymphocyte proliferation and represented the mean ± SEM of three independent experiments. *: $p < 0.05$, ****: $p < 0.0001$, one-way ANOVA and Tukey's multiple comparison test.

B. S5505 Fumed silica nanoparticles increased T-cell proliferation at all DC:T-cell tested ratios. Cells were incubated with 12.5 µg.mL^{-1} of S5505 fumed silica nanoparticles for 16 hours. LPS and PHA were used as positive controls. Treated moDC were co-cultured with allogeneic CD4+ T-cells loaded with CFSE at different ratios: 1:100 (1 moDC per 100 T-cells), 1:50 (1 moDC for 50 T-cells) and 1:20 (1 moDC for 20 T-cells). Proliferation was measured after 5 days of co-culture as the percentage of CFSE^{low} CD4+ T-cells. Untreated moDCs were used as control. Results were expressed as a percentage of increase in lymphocyte proliferation and represented the mean ± SEM of three independent experiments. **: $p < 0.01$, two-way ANOVA and Sidak's multiple comparison test.

3.7. S5505 Fumed silica nanoparticles increased the production of IL-9 and IL-17A/F by CD4+ T-cells

To get insight into the mechanism of the CD4+ T-cell response, we next analyzed the production of T-cell cytokines in the co-culture supernatants (Figure 6). Results showed that when moDCs were exposed to 12.5 µg.mL^{-1} of S5505 fumed silica NPs, the production of IL-9, IL-17A, and IL-17F in the supernatant of co-cultures was significantly augmented. Moreover, an increase in IL-5 production was also observed but was non-significant due to the high variability of the results. IFN-γ, IL-22, and IL-13 were also augmented but the levels were also not statistically different from controls. Interestingly, SAS-NPs caused a more significant production of IL-9 than LPS (figure 6).

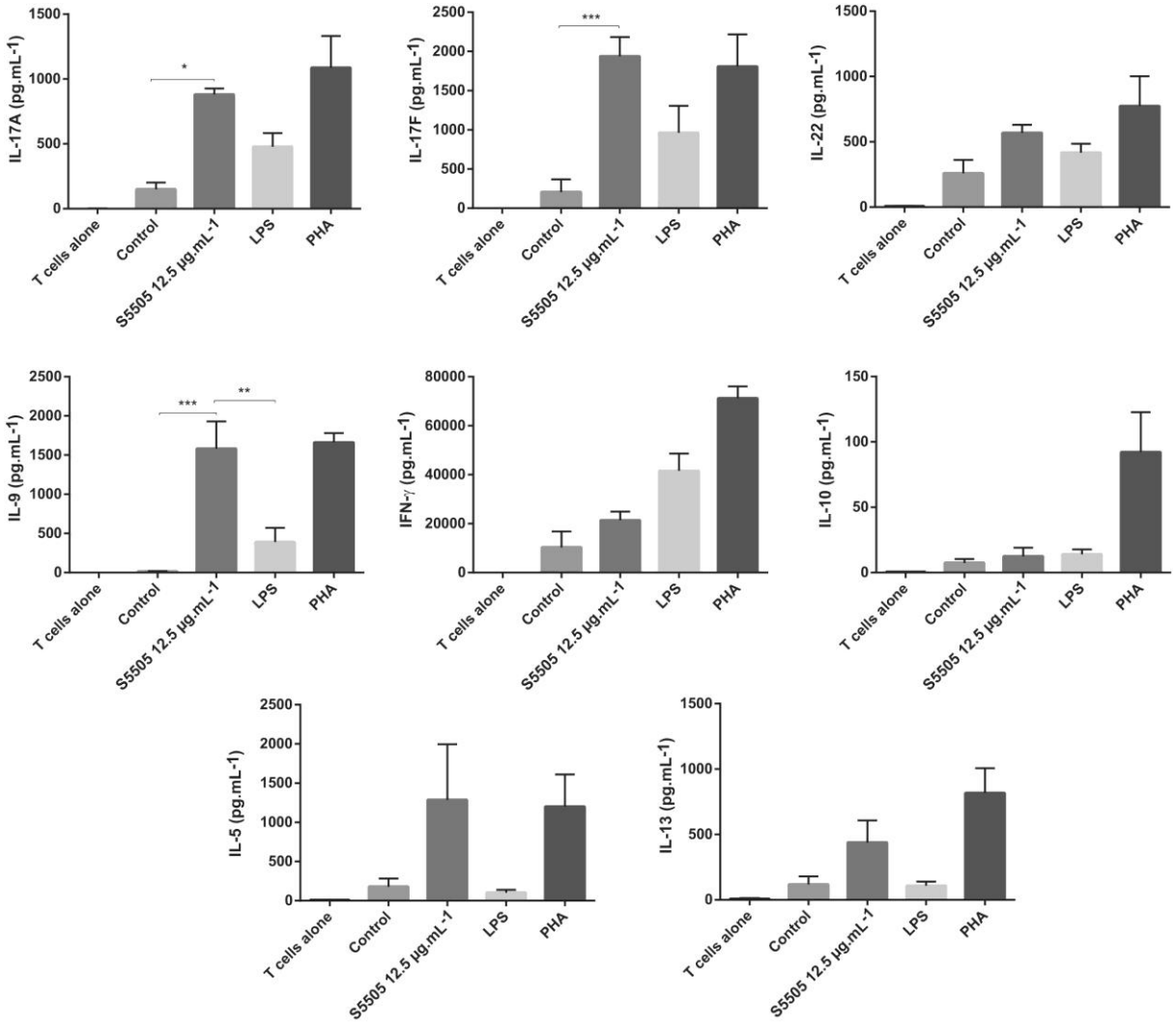

Figure 6. S5505 Fumed silica nanoparticles increased the production of IL-9 and IL-17A/F by CD4+ T-cells

Cells were incubated with 12.5 µg.mL^{-1} of S5505 fumed silica nanoparticles for 16 hours. LPS and PHA were used as positive controls. Treated moDCs were co-cultured with allogeneic CD4+ T-cells loaded at a ratio of 1 moDC for 20 CD4+ T-cells. On day 5, cytokines levels were measured in co-culture supernatants using U-PLEX MSD technology. Untreated moDCs were used as control. Results were expressed in the quantity of detected cytokines (pg.mL^{-1}) and represented the mean ± SEM of three independent experiments. *: $p < 0.05$, **: $p < 0.01$, ***: $p < 0.001$ one-way ANOVA and Tukey's multiple comparison test.

4. Discussion

As a first-line defense against non-self-entities, DCs are sentinels of the immune system, actively sampling the antigenic environment and sensing danger. The "danger theory" explains how immune responses could take place in aseptic conditions (Matzinger 1994). Among the patterns sounding the alarm, Gallo and Gallucci proposed the NAMPs (Gallo and Gallucci 2013). Nanomaterials may be considered as "emerging" danger signals activating DCs either directly or indirectly as a result of cell injury (Gallo and Gallucci 2013; Pallardy et al. 2017), enabling them to undergo a full maturation process and to migrate to regional lymph nodes and activate naive T-lymphocytes (Pallardy et al. 2017). Our results suggested that human DCs could sense SAS-NPs as danger signals, potentially altering the immunogenicity of environmental antigens (Shannahan and Brown 2014). Indeed, as previously described for air pollution particles (de Haar et al. 2008), there is increasing evidence for

the impact of nanomaterials on allergic airway disease (Meldrum et al. 2017) and skin sensitization (Yoshioka et al. 2017). While only a few *in vivo* studies explored to date the danger signal hypothesis for SAS-NPs, their results comfort our *in vitro* observations (Brandenberger et al. 2013; Han et al. 2016). However, significant gaps remain concerning the effects of nanomaterials on DCs, and the relevance of the selected experimental models for humans.
The effects of different nanoparticles including Micromod® colloidal silica (Hirai et al. 2012; Nakanishi et al. 2016), Sigma "ultrafine" silica (Kang and Lim 2012) or Aerosil 380F and 200 F (Winkler et al. 2017) have been previously studied using the murine BMDCs. Most studies examined the DCs phenotype, with a large variety of markers (CD40, CD69, CD80, CD86, MHC II, ..) and the production of pro-inflammatory cytokines (Heng et al. 2011; Zhu et al. 2014) has not yet been extensively studied. This approach would benefit from more functional tests such as DCs migration assays (Li et al. 2010) or allogeneic co-culture to explore the ability of activated DCs to induce T-cell proliferation (Koike et al. 2008). Moreover, the extrapolation of these results to humans remains challenging and some investigators decided to use human DC obtained from either CD34+ progenitor cells or monocytes (Andersson-Willman et al. 2012; Barillet et al. 2019; Laverny et al. 2013; Schanen et al. 2013; Vandebriel et al. 2018). The effects of silica NPs on human DCs have been thoroughly explored for mesoporous silica particles (Kupferschmidt et al. 2014; Vallhov et al. 2007; Vallhov et al. 2012), known to display a unique pore structure and extremely large surface area, making them suitable for drug and vaccine delivery systems. Our work is part of a different approach addressing the immunotoxic effects of unintentional, passive exposure to SAS-NPs used in consumer products or industry, such as fumed or colloidal silica. To this end, our experiments were designed to propose a robust *in vitro* model of human innate immune responsiveness using primary DCs. We specifically explored NPs impact on human DCs using an integrated *in vitro* model able to measure the DCs phenotype alterations following SAS-NPs exposure but also the consequences of such alterations on T-cell responses.

The criteria to identify danger signals comprise DCs activation and maturation and the ability to regulate their migratory properties. In our study, DCs maturation was clearly evidenced by phenotypical modifications of human moDCs with increased expression of CD83, CD86, and CXCR4 on the cell surface, a feature which appears common to all the SAS-NPs we tested. CD83 is a membrane-bound glycoprotein considered one of the hallmarks of fully matured DCs (Prechtel and Steinkasserer 2007) while CXCR4 binds the CXCL12 chemokine that plays a role in mature DCs migration through the afferent lymphatic vessels to the lymph nodes (Pozzobon et al. 2016). SAS-NPs-induced moDCs activation was further supported by an increase in the secretion of pro-inflammatory cytokines, particularly CXCL-8 and CXCL-12, again for all the pyrogenic and colloidal silica tested. These phenotypical modifications are unlikely due to contamination by LPS since the SAS-NPs used did not contain detectable levels of endotoxins, as verified using the LAL test (Li et al. 2017). Using human moDCs, Vallhov *et al.* tested mesoporous silica calcinated AMS-6 nano- and AMS-8 microparticles and found a slight but significant increase of CD86, no significant effect on CD83 and MHC II expression, and a reduced expression of the CD40 and CD80 costimulatory molecules (Vallhov et al. 2007). The conclusion was that mesoporous silica modified DCs phenotype in a relatively immature state confirmed later with the SBA-15 mesoporous silica particles (Vallhov et al. 2012). These contrasting effects can be attributed to the distinct characteristics of the silica NPs tested. Indeed, Winter *et al.* demonstrated on murine BMDCs that fumed silica NPs, which seem comparable to S5505 in terms of physico-chemical characteristics, significantly increased the expression of MHC II as well as CD80 and CD86 (Winter et al. 2011). More recently, Winkler *et al.* suggested that high concentrations of pyrogenic SAS-NPs could activate BMDCs with a weak but non-significant upregulation of CD40 and CD86 expressions and release of IL-1β and TNF-α (Winkler et al. 2017). The ability of SAS-NPs to increase the release of pro-inflammatory cytokines such as IL-6 and CXCL-8 was previously demonstrated on human epithelial cell lines (Gualtieri et al. 2012; Hetland et al. 2001). In the RAW 264.7 macrophage-like cell line, SAS-NPs increase the gene expression of *IL-1*, *IL-6* and *TNF-α* (Park and Park 2009) or the persistent production of IL-6 and TNF-α (Torres et al. 2020).

We then explored by TEM the ability of human DCs to internalize SAS-NPs. Our work shows for the first time the internalization of 25 $\mu g.mL^{-1}$ S5505 fumed silica in human DCs within 24h. As

intracellular nanoparticles were only seen in cytoplasmic vesicles, this suggests endocytosis processes. Considering the observation of *ca* 100 different cell sections per condition, it seems that NPs-treated cells present more dendrites than control cells, in agreement with their maturation. Consistent with our results, the presence of fumed silica NPs clusters was demonstrated at the plasma membrane and in endosome-like vesicles in BMDCs, for 250 $\mu g.mL^{-1}$ SAS-NPs concentration (Winkler et al. 2017). In MoDCs, the internalization of mesoporous silica was also observed (Vallhov et al. 2012).

The term "mature" is commonly used as a phenotypic rather than a functional state, designating DCs expressing high levels of maturation and co-stimulation molecules on their surface. However, phenotypically mature DCs do not always promote T-cell immunity (Reis e Sousa 2006). The ultimate consequence of functional DCs maturation for the immune response is T-cell activation and proliferation, only possible after productive interaction with activated DCs. We then addressed the consequences of SAS-NPs-induced DCs phenotype alterations on T-lymphocytes activation using an allogeneic DC:T-cell co-culture model. Our results showed a strong augmentation of T-cell proliferation when moDCs were stimulated with S5505 fumed silica NPs. Interestingly, this effect was comparable to LPS, a well-known danger signal. This increase in T-cell proliferation was accompanied by an increase in T-cell cytokine secretion, notably IL-17A/F and IL-9. IL-5 was also increased but in a non-significant manner. These results are consistent with the pro-inflammatory phenotype of DCs described above and with the danger signal hypothesis. The production of such cytokines suggested that these activated T-cells could preferentially adopt a Th2 and Th17 orientation, but this remains to be confirmed by performing intracellular cytokine measurements. There are only few studies in the literature using co-culture of T-cells and DCs to assess the functional DCs maturation in presence of NPs (Barillet et al. 2019; Schanen et al. 2013; Vallhov et al. 2012; Yang et al. 2010) but these results strongly supported the observations of phenotypic alterations. Those conducted on carbon black (Koike et al. 2008) and CeO_2/TiO_2 NPs (Schanen et al. 2013) suggested that these nanomaterials could drive the polarization of the T-cell response, but experiments specifically designed to explore T-cells polarization would be needed. Vallhov *et al.* conducted an elaborated autologous co-culture experiment using naive CD4+ T lymphocytes with anti-CD3 stimulation on day 7 (Vallhov et al. 2012). They showed that mesoporous SAS-NPs SBA-15 could drive T-cell polarization with IFN-γ, IL-4, and IL-13 production, highlighting the adjuvant effect of this material and the interest to explore the DC:T-cell interaction. In our study, the allogeneic co-culture experiments were designed to specifically address the functional maturation of DCs, which expressed high surface levels of CD83 and CD86 molecules and produced cytokines.

Remarkably, pyrogenic or colloidal NPs induced the maturation of human DCs by regulating the expression of the same markers and the production of the same pro-inflammatory cytokines. It would be interesting to identify the characteristics responsible for these common immunotoxic properties, such as the silanol groups and siloxane rings. Reducing their surface expression has been demonstrated to decrease fumed silica NPs cytotoxic effects in THP-1 cells (Sun et al. 2015). A major role was attributed to their concentration (Zhang et al. 2012) and specific surface arrangement in biological membranes damages (Pavan et al. 2013), closely linked to the initiation of inflammatory reactions and IL-1 release (Pavan et al. 2014). Recently, the "nearly free silanols", in their repartition and local density, were presented as key molecular moieties in silica toxicity (Pavan et al. 2019; Pavan et al. 2020). Although controversial, the generation of reactive oxygen species (ROS) by SAS-NPs could contribute to membrane damage (Di Cristo et al. 2016; Sun et al. 2015; Zhang et al. 2012). Strained siloxane rings of fumed silica, absent in colloidal silicas, could be the precursors of hydroxyl radicals (Zhang et al. 2012). Zhang *et al* found higher toxicity of fumed silica NPs compared to "Stöber" colloidal silica in epithelial and macrophage cells (Zhang et al. 2012). In our experiments, the concentrations of Ludox® TMA leading to DCs activation were higher than those of fumed silica, but we found nevertheless comparable immunotoxic effects.

In conclusion, recent studies have challenged the assumed biocompatibility of SAS-NPs, particularly with immune cells (Himly et al. 2017; Mocan et al. 2016; Shannahan and Brown 2014), suggesting that a comprehensive evaluation of their actual immunotoxicity must be carried out. In this work, we demonstrated using human DCs that SAS-NPs promoted the two first steps of adaptive immune response by increasing the maturation of human DCs and augmenting allogeneic T-lymphocyte response, characterized by increased proliferation and cytokine secretion. Given their effects on DCs

activation, SAS-NPS may therefore play a role in the immunization process against environmental antigens, in situations where simultaneous exposure with nanoparticles could occur in the workplace, as well as in everyday life.

List of abbreviations

SAS-NPs: Synthetic amorphous silica nanoparticles; DCs: dendritic cells; moDCs: monocyte-derived dendritic cells; BMDCs: bone marrow-derived dendritic cells; MHC II: major histocompatibility complex class II; LPS: lipopolysaccharide; PHA: phytohaemagglutinin; DLS: dynamic light scattering; LAL: Limulus amebocyte lysate; PBMC: peripheral blood mononuclear cells; PI: propidium iodide; CFSE: carboxyfluorescein succinimidyl ester.

Data links

Not applicable.

Conflicts of Interest (COI)

The authors declare that they have no conflicts of interest.

Funding

The French National Research Program for Environmental and Occupational Health of ANSES funded the study (PNREST 2015/032, Silimmun Grant). Alexia Feray is a recipient of a LERMIT (Laboratoire d'excellence en recherche sur le médicament et l'innovation thérapeutique) PhD fellowship.

Acknowledgments

Alexia Feray and Eléonore Guillet were master fellows of DIM QI2 (Réseau de recherche Qualité de l'air en Ile-de-France). The present work has benefited from the CYTOMETRY / ELECTRONIC MICROSCOPY / LIGHT MICROSCOPY facility of Imagerie- Gif, (http://www.i2bc.paris-saclay.fr), member of IBiSA (http://www.ibisa.net), supported by "France- BioImaging" (ANR- 10- INBS- 04- 01), and the Labex "Saclay Plant Sciences" (ANR-10-LABX-0040-SPS). The authors thank Eugénie Deschamps for her help in the characterization of NM-202 nanoparticles. They warmly acknowledge Dr. Vanessa Lievin-Le Moal for the microbiological tests of nanoparticles and Dr. Eric Finster for his careful reading and English corrections of the revised manuscript.

References

Andersson-Willman B, Gehrmann U, Cansu Z, Buerki-Thurnherr T, Krug HF, Gabrielsson S, Scheynius A. 2012. Effects of subtoxic concentrations of tio2 and zno nanoparticles on human lymphocytes, dendritic cells and exosome production. Toxicol Appl Pharmacol. 264(1):94-103.

Arts JH, Muijser H, Duistermaat E, Junker K, Kuper CF. 2007. Five-day inhalation toxicity study of three types of synthetic amorphous silicas in wistar rats and post-exposure evaluations for up to 3 months. Food Chem Toxicol. 45(10):1856-1867.

Barillet S, Fattal E, Mura S, Tsapis N, Pallardy M, Hillaireau H, Kerdine-Romer S. 2019. Immunotoxicity of poly (lactic-co-glycolic acid) nanoparticles: Influence of surface properties on dendritic cell activation. Nanotoxicology. 13(5):606-622.

Brandenberger C, Rowley NL, Jackson-Humbles DN, Zhang Q, Bramble LA, Lewandowski RP, Wagner JG, Chen W, Kaplan BL, Kaminski NE et al. 2013. Engineered silica nanoparticles act as adjuvants to enhance allergic airway disease in mice. Part Fibre Toxicol. 10:26.

Croissant JG, Butler KS, Zink JI, Brinker CJ. 2020. Synthetic amorphous silica nanoparticles: Toxicity, biomedical and environmental implications. Nature Reviews Materials. 5(12):886-909.

de Haar C, Kool M, Hassing I, Bol M, Lambrecht BN, Pieters R. 2008. Lung dendritic cells are stimulated by ultrafine particles and play a key role in particle adjuvant activity. J Allergy Clin Immunol. 121(5):1246-1254.

Di Cristo L, Movia D, Bianchi MG, Allegri M, Mohamed BM, Bell AP, Moore C, Pinelli S, Rasmussen K, Riego-Sintes J et al. 2016. Proinflammatory effects of pyrogenic and precipitated amorphous silica nanoparticles in innate immunity cells. Toxicol Sci. 150(1):40-53.

Doi K. 1982. Structure changes in amorphous silica by neutron-irradiation. J Non-Cryst Solids. 51(3):367-380.

Fadeel B. 2012. Clear and present danger? Engineered nanoparticles and the immune system. Swiss Med Wkly. 142:w13609.

Farrera C, Fadeel B. 2015. It takes two to tango: Understanding the interactions between engineered nanomaterials and the immune system. Eur J Pharm Biopharm. 95(Pt A):3-12.

Feray A, Szely N, Guillet E, Hullo M, Legrand FX, Brun E, Pallardy M, Biola-Vidamment A. 2020. How to address the adjuvant effects of nanoparticles on the immune system. Nanomaterials (Basel). 10(3).

Gallo PM, Gallucci S. 2013. The dendritic cell response to classic, emerging, and homeostatic danger signals. Implications for autoimmunity. Front Immunol. 4:138.

Gualtieri M, Skuland T, Iversen TG, Lag M, Schwarze P, Bilanicova D, Pojana G, Refsnes M. 2012. Importance of agglomeration state and exposure conditions for uptake and pro-inflammatory responses to amorphous silica nanoparticles in bronchial epithelial cells. Nanotoxicology. 6(7):700-712.

Gustafson HH, Holt-Casper D, Grainger DW, Ghandehari H. 2015. Nanoparticle uptake: The phagocyte problem. Nano Today. 10(4):487-510.

Han H, Park YH, Park HJ, Lee K, Um K, Park JW, Lee JH. 2016. Toxic and adjuvant effects of silica nanoparticles on ovalbumin-induced allergic airway inflammation in mice. Respir Res. 17(1):60.

Heng BC, Zhao X, Tan EC, Khamis N, Assodani A, Xiong S, Ruedl C, Ng KW, Loo JS. 2011. Evaluation of the cytotoxic and inflammatory potential of differentially shaped zinc oxide nanoparticles. Arch Toxicol. 85(12):1517-1528.

Hetland RB, Schwarze PE, Johansen BV, Myran T, Uthus N, Refsnes M. 2001. Silica-induced cytokine release from a549 cells: Importance of surface area versus size. Hum Exp Toxicol. 20(1):46-55.

Himly M, Mills-Goodlet R, Geppert M, Duschl A. 2017. Nanomaterials in the context of type 2 immune responses-fears and potentials. Front Immunol. 8:471.

Hirai T, Yoshioka Y, Takahashi H, Ichihashi K, Yoshida T, Tochigi S, Nagano K, Abe Y, Kamada H, Tsunoda S et al. 2012. Amorphous silica nanoparticles enhance cross-presentation in murine dendritic cells. Biochem Biophys Res Commun. 427(3):553-556.

Hopken UE, Lehmann I, Droese J, Lipp M, Schuler T, Rehm A. 2005. The ratio between dendritic cells and t cells determines the outcome of their encounter: Proliferation versus deletion. Eur J Immunol. 35(10):2851-2863.

Jani P, Halbert GW, Langridge J, Florence AT. 1990. Nanoparticle uptake by the rat gastrointestinal mucosa: Quantitation and particle size dependency. J Pharm Pharmacol. 42(12):821-826.

Kang K, Lim JS. 2012. Induction of functional changes of dendritic cells by silica nanoparticles. Immune Netw. 12(3):104-112.

Koike E, Takano H, Inoue K, Yanagisawa R, Kobayashi T. 2008. Carbon black nanoparticles promote the maturation and function of mouse bone marrow-derived dendritic cells. Chemosphere. 73(3):371-376.

Kupferschmidt N, Qazi KR, Kemi C, Vallhov H, Garcia-Bennett AE, Gabrielsson S, Scheynius A. 2014. Mesoporous silica particles potentiate antigen-specific t-cell responses. Nanomedicine (Lond). 9(12):1835-1846.

Laverny G, Casset A, Purohit A, Schaeffer E, Spiegelhalter C, de Blay F, Pons F. 2013. Immunomodulatory properties of multi-walled carbon nanotubes in peripheral blood mononuclear cells from healthy subjects and allergic patients. Toxicol Lett. 217(2):91-101.
Li A, Qin L, Zhu D, Zhu R, Sun J, Wang S. 2010. Signalling pathways involved in the activation of dendritic cells by layered double hydroxide nanoparticles. Biomaterials. 31(4):748-756.
Li Y, Fujita M, Boraschi D. 2017. Endotoxin contamination in nanomaterials leads to the misinterpretation of immunosafety results. Front Immunol. 8:472.
Lutz MB, Schuler G. 2002. Immature, semi-mature and fully mature dendritic cells: Which signals induce tolerance or immunity? Trends Immunol. 23(9):445-449.
Matzinger P. 1994. Tolerance, danger, and the extended family. Annu Rev Immunol. 12:991-1045.
Meldrum K, Guo C, Marczylo EL, Gant TW, Smith R, Leonard MO. 2017. Mechanistic insight into the impact of nanomaterials on asthma and allergic airway disease. Part Fibre Toxicol. 14(1):45.
Mocan T, Matea CT, Iancu C, Agoston-Coldea L, Mocan L, Orasan R. 2016. Hypersensitivity and nanoparticles: Update and research trends. Clujul Med. 89(2):216-219.
Monopoli MP, Walczyk D, Campbell A, Elia G, Lynch I, Bombelli FB, Dawson KA. 2011. Physical-chemical aspects of protein corona: Relevance to in vitro and in vivo biological impacts of nanoparticles. J Am Chem Soc. 133(8):2525-2534.
Nakanishi K, Tsukimoto M, Tanuma S, Takeda K, Kojima S. 2016. Silica nanoparticles activate purinergic signaling via p2x7 receptor in dendritic cells, leading to production of pro-inflammatory cytokines. Toxicol In Vitro. 35:202-211.
Napierska D, Thomassen LC, Lison D, Martens JA, Hoet PH. 2010. The nanosilica hazard: Another variable entity. Part Fibre Toxicol. 7(1):39.
Pallardy MJ, Turbica I, Biola-Vidamment A. 2017. Why the immune system should be concerned by nanomaterials? Front Immunol. 8:544.
Park EJ, Park K. 2009. Oxidative stress and pro-inflammatory responses induced by silica nanoparticles in vivo and in vitro. Toxicol Lett. 184(1):18-25.
Pavan C, Delle Piane M, Gullo M, Filippi F, Fubini B, Hoet P, Horwell CJ, Huaux F, Lison D, Lo Giudice C et al. 2019. The puzzling issue of silica toxicity: Are silanols bridging the gaps between surface states and pathogenicity? Part Fibre Toxicol. 16(1):32.
Pavan C, Rabolli V, Tomatis M, Fubini B, Lison D. 2014. Why does the hemolytic activity of silica predict its pro-inflammatory activity? Part Fibre Toxicol. 11:76.
Pavan C, Santalucia R, Leinardi R, Fabbiani M, Yakoub Y, Uwambayinema F, Ugliengo P, Tomatis M, Martra G, Turci F et al. 2020. Nearly free surface silanols are the critical molecular moieties that initiate the toxicity of silica particles. Proc Natl Acad Sci U S A. 117(45):27836-27846.
Pavan C, Tomatis M, Ghiazza M, Rabolli V, Bolis V, Lison D, Fubini B. 2013. In search of the chemical basis of the hemolytic potential of silicas. Chem Res Toxicol. 26(8):1188-1198.
Pozzobon T, Goldoni G, Viola A, Molon B. 2016. Cxcr4 signaling in health and disease. Immunology Letters. 177:6-15.
Pradeu T, Cooper EL. 2012. The danger theory: 20 years later. Front Immunol. 3:287.
Prechtel AT, Steinkasserer A. 2007. Cd83: An update on functions and prospects of the maturation marker of dendritic cells. Arch Dermatol Res. 299(2):59-69.
Reis e Sousa C. 2006. Dendritic cells in a mature age. Nat Rev Immunol. 6(6):476-483.
Sccs, Hoet PH. 2016. Opinion of the scientific committee on consumer safety (sccs) - revision of the opinion on the safety of the use of silica, hydrated silica, and silica surface modified with alkyl silylates (nano form) in cosmetic products. Regul Toxicol Pharmacol. 74:79-80.
Schanen BC, Das S, Reilly CM, Warren WL, Self WT, Seal S, Drake DR, 3rd. 2013. Immunomodulation and t helper th(1)/th(2) response polarization by ceo(2) and tio(2) nanoparticles. PLoS One. 8(5):e62816.
Schindelin J, Arganda-Carreras I, Frise E, Kaynig V, Longair M, Pietzsch T, Preibisch S, Rueden C, Saalfeld S, Schmid B et al. 2012. Fiji: An open-source platform for biological-image analysis. Nat Methods. 9(7):676-682.
Shannahan JH, Brown JM. 2014. Engineered nanomaterial exposure and the risk of allergic disease. Curr Opin Allergy Clin Immunol. 14(2):95-99.

Sun B, Pokhrel S, Dunphy DR, Zhang H, Ji Z, Wang X, Wang M, Liao YP, Chang CH, Dong J et al. 2015. Reduction of acute inflammatory effects of fumed silica nanoparticles in the lung by adjusting silanol display through calcination and metal doping. ACS Nano. 9(9):9357-9372.

Sun B, Wang X, Liao YP, Ji Z, Chang CH, Pokhrel S, Ku J, Liu X, Wang M, Dunphy DR et al. 2016. Repetitive dosing of fumed silica leads to profibrogenic effects through unique structure-activity relationships and biopersistence in the lung. ACS Nano. 10(8):8054-8066.

Tan JK, O'Neill HC. 2005. Maturation requirements for dendritic cells in t cell stimulation leading to tolerance versus immunity. J Leukoc Biol. 78(2):319-324.

Torres A, Dalzon B, Collin-Faure V, Diemer H, Fenel D, Schoehn G, Cianferani S, Carriere M, Rabilloud T. 2020. How reversible are the effects of fumed silica on macrophages? A proteomics-informed view. Nanomaterials (Basel). 10(10).

Vallhov H, Gabrielsson S, Stromme M, Scheynius A, Garcia-Bennett AE. 2007. Mesoporous silica particles induce size dependent effects on human dendritic cells. Nano Lett. 7(12):3576-3582.

Vallhov H, Kupferschmidt N, Gabrielsson S, Paulie S, Stromme M, Garcia-Bennett AE, Scheynius A. 2012. Adjuvant properties of mesoporous silica particles tune the development of effector t cells. Small. 8(13):2116-2124.

Vandebriel RJ, Vermeulen JP, van Engelen LB, de Jong B, Verhagen LM, de la Fonteyne-Blankestijn LJ, Hoonakker ME, de Jong WH. 2018. The crystal structure of titanium dioxide nanoparticles influences immune activity in vitro and in vivo. Part Fibre Toxicol. 15(1):9.

Winkler HC, Kornprobst J, Wick P, von Moos LM, Trantakis I, Schraner EM, Bathke B, Hochrein H, Suter M, Naegeli H. 2017. Myd88-dependent pro-interleukin-1beta induction in dendritic cells exposed to food-grade synthetic amorphous silica. Part Fibre Toxicol. 14(1):21.

Winkler HC, Suter M, Naegeli H. 2016. Critical review of the safety assessment of nano-structured silica additives in food. J Nanobiotechnology. 14(1):44.

Winter M, Beer HD, Hornung V, Kramer U, Schins RP, Forster I. 2011. Activation of the inflammasome by amorphous silica and tio2 nanoparticles in murine dendritic cells. Nanotoxicology. 5(3):326-340.

Worbs T, Hammerschmidt SI, Forster R. 2017. Dendritic cell migration in health and disease. Nat Rev Immunol. 17(1):30-48.

Yang D, Zhao Y, Guo H, Li Y, Tewary P, Xing G, Hou W, Oppenheim JJ, Zhang N. 2010. [gd@c(82)(oh)(22)](n) nanoparticles induce dendritic cell maturation and activate th1 immune responses. ACS Nano. 4(2):1178-1186.

Yoshioka Y, Kuroda E, Hirai T, Tsutsumi Y, Ishii KJ. 2017. Allergic responses induced by the immunomodulatory effects of nanomaterials upon skin exposure. Front Immunol. 8:169.

Younes M, Aggett P, Aguilar F, Crebelli R, Dusemund B, Filipič M, Frutos MJ, Galtier P, Gott D, Gundert- Remy U et al. 2018. Re- evaluation of silicon dioxide (e 551) as a food additive. EFSA Journal. 16(1).

Zhang H, Dunphy DR, Jiang X, Meng H, Sun B, Tarn D, Xue M, Wang X, Lin S, Ji Z et al. 2012. Processing pathway dependence of amorphous silica nanoparticle toxicity: Colloidal vs pyrolytic. J Am Chem Soc. 134(38):15790-15804.

Zhu R, Zhu Y, Zhang M, Xiao Y, Du X, Liu H, Wang S. 2014. The induction of maturation on dendritic cells by tio2 and fe(3)o(4)@tio(2) nanoparticles via nf-kappab signaling pathway. Mater Sci Eng C Mater Biol Appl. 39:305-314.

Supplementary figures

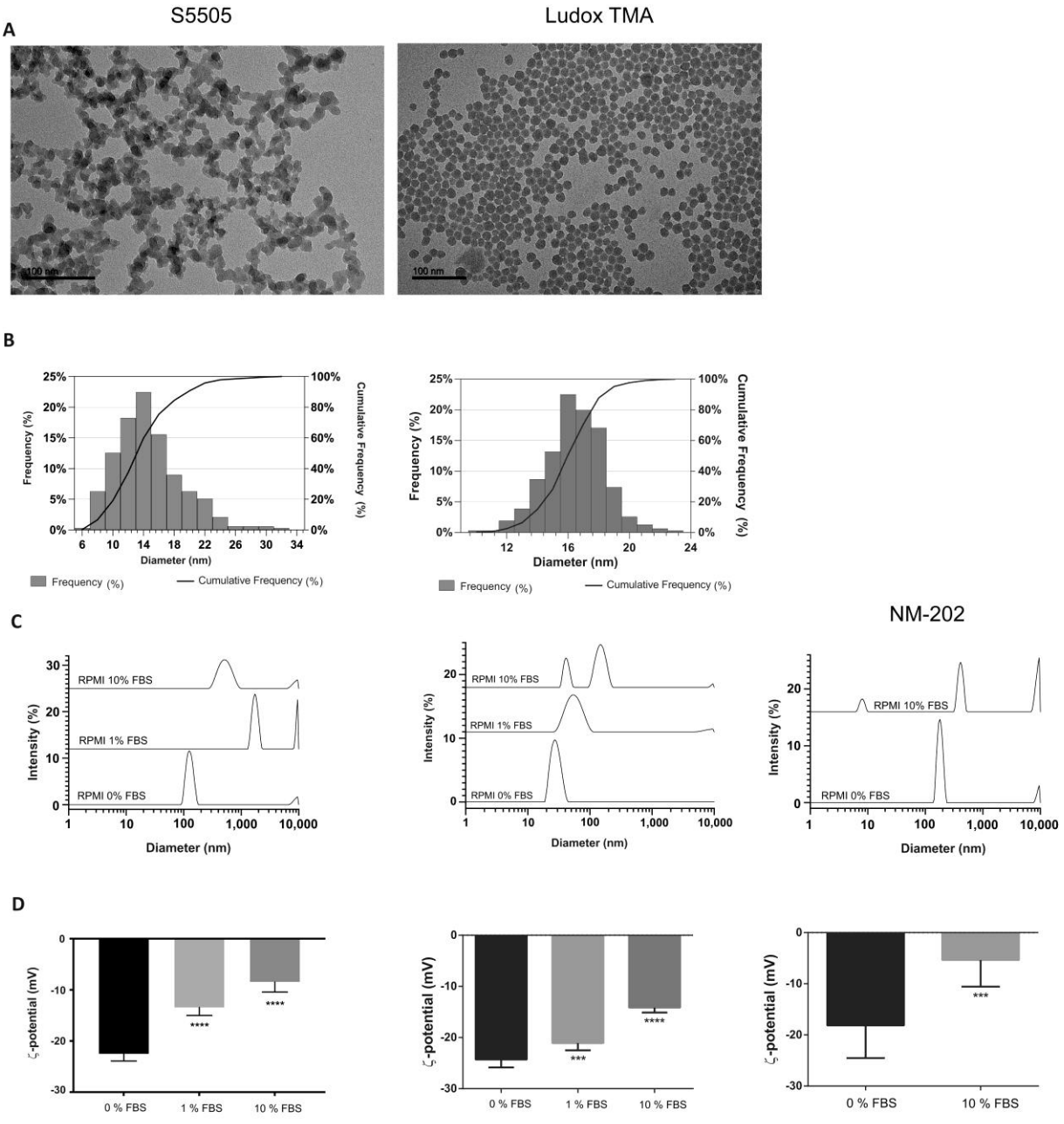

Figure S1. Characterization of synthetic amorphous silica nanoparticles.

A. Typical TEM image of unstained S5505 fumed silica or Ludox® TMA nanoparticles suspended in water.
B. Distribution histogram and cumulative distribution of the constituent nanoparticle size determined by TEM (total count: 334 particles for S5505 and 311 for Ludox® TMA).
C. Intensity-weighted size distribution profiles of S5505 fumed silica, Ludox® TMA or NM-202 nanoparticles in pure RPMI 1640, in RPMI 1640 supplemented with 1% of Fetal Bovine Serum and in RPMI 1640 supplemented with 10% of Fetal Bovine Serum were obtained using Dynamic Light Scattering. Each measure was repeated ten times.
D. Zeta-potential variations of S5505 fumed silica nanoparticles, Ludox® TMA or NM-202 in RPMI 1640 with or without fetal bovine serum (zeta-potential data are represented as mean ± SD of ten independent measurements).
****: $p < 0.0001$, one-way ANOVA and Tukey's multiple comparison test.

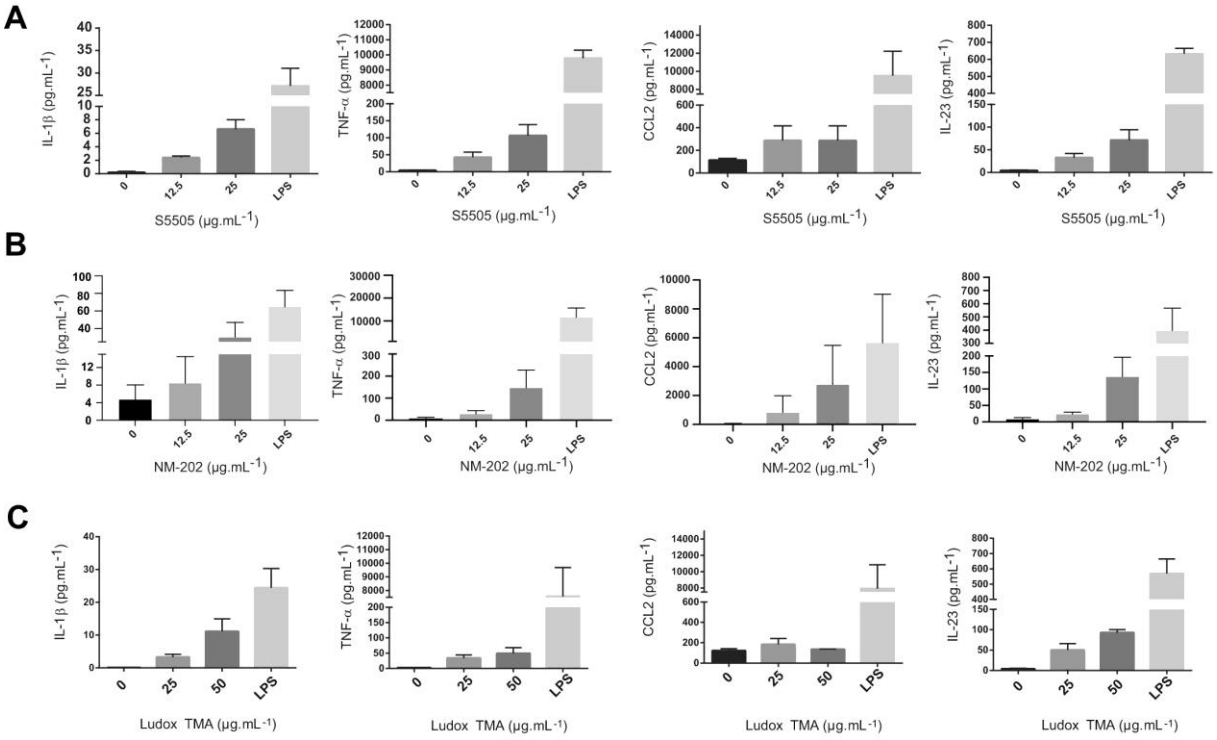

Figure S2. Synthetic amorphous silica nanoparticles induced moDCs inflammatory cytokines and chemokines secretion.

Cells were incubated with 12.5 and 25 µg.mL^{-1} of S5505 fumed silica nanoparticles (A) or NM-202 (B) or Ludox® TMA (C) for 16 hours. LPS was used as a positive control. The moDCs culture supernatants were collected and analyzed using U-PLEX MSD technology. Unloaded moDCs were used as control. Results were expressed in the quantity of detected cytokines (pg.mL^{-1}) and represented the mean ± SEM of three independent experiments. **: $p < 0.01$, ***: $p < 0.001$, ****: $p < 0.0001$, one-way ANOVA and Tukey's multiple comparison test (statistics for LPS are not shown).